Infrared spectroscopy of neutral water clusters at finite temperature: Evidence for a noncyclic pentamer

Bingbing Zhang[a,1], Yong Yu[a,b,1], Yang-Yang Zhang[c,1], Shukang Jiang[a,b], Qinming Li[a,b], Han-Shi Hu[c], Gang Li[a], Zhi Zhao[a], Chong Wang[a], Hua Xie[a], Weiqing Zhang[a], Dongxu Dai[a], Guorong Wu[a], Dong H. Zhang[a], Ling Jiang[a,2], Jun Li (李 隽)[c,d,2], and Xueming Yang[a,d,2]

[a]State Key Laboratory of Molecular Reaction Dynamics, Dalian Institute of Chemical Physics, Chinese Academy of Sciences, 116023 Dalian, China; [b]University of Chinese Academy of Sciences, 100049 Beijing, China; [c]Department of Chemistry, Key Laboratory of Organic Optoelectronics and Molecular Engineering of the Ministry of Education, Tsinghua University, 100084 Beijing, China; and [d]Department of Chemistry, College of Science, Southern University of Science and Technology, 518055 Shenzhen, China

Edited by Robert W. Field, Massachusetts Institute of Technology, Cambridge, MA, and approved May 14, 2020 (received for review January 11, 2020)

Infrared spectroscopic study of neutral water clusters is crucial to understanding of the hydrogen-bonding networks in liquid water and ice. Here we report infrared spectra of size-selected neutral water clusters, $(H_2O)_n$ (n = 3–6), in the OH stretching vibration region, based on threshold photoionization using a tunable vacuum ultraviolet free-electron laser. Distinct OH stretch vibrational fundamentals observed in the 3,500–3,600-cm^{-1} region of $(H_2O)_5$ provide unique spectral signatures for the formation of a noncyclic pentamer, which coexists with the global-minimum cyclic structure previously identified in the gas phase. The main features of infrared spectra of the pentamer and hexamer, $(H_2O)_n$ (n = 5 and 6), span the entire OH stretching band of liquid water, suggesting that they start to exhibit the richness and diversity of hydrogen-bonding networks in bulk water.

water cluster | infrared spectroscopy | hydrogen bonding | free-electron laser

As one of the most important matters on the earth, water and its interactions with other substances are essential in human life. However, understanding the structure of liquid water and its hydrogen-bonding networks remains a grand challenge. Spectroscopic investigation of gas-phase water clusters and its transition to bulk liquid water is critical in understanding the structures and properties of condensed-phase water (1–3). Here, we present a technique for infrared (IR) spectra of size-selected neutral water clusters based on threshold photoionization using a tunable vacuum ultraviolet free-electron laser. It is found that noncyclic three-dimensional (3D) structure of water clusters begins to exist already at the pentamer with low finite temperature.

On the one hand, cationic or anionic forms of water clusters have been extensively investigated because of relatively easy size selection and detection. For the protonated water clusters, $H^+(H_2O)_n$, small-sized clusters prefer chain- or treelike networks, closed net motifs are formed at n = 10, and hydrogen-bonding networks evolve into closed cage structures at n = 21 (4–6). It was found that the Eigen $[H_3O^+\cdots(H_2O)_3]$ and Zundel $(H_2O\cdots H^+\cdots OH_2)$ motifs play important roles in the proton accommodation in water (4–11). Experimental studies of anionic water clusters were devoted to understanding the nature of the excess electron in water (12–16). These studies provide important knowledge on the structures and dynamics of the ionic water clusters. On the other hand, hydrogen-bonding network structures in neutral water clusters are substantially different from those in ionic water clusters. Therefore, it is more relevant to investigate the hydrogen-bonding networks of confinement-free neutral water clusters to gain deeper insights into the evolution of hydrogen-bonding networks from small clusters to liquid water. Unfortunately, it is even more challenging experimentally to investigate size-specific neutral water clusters due to difficult size selection for neutral clusters in general.

Over the past several decades, various experimental techniques were developed to study the neutral water clusters in the mid-IR and far-IR regions. The gas-phase mid-IR spectrum of water dimer in the OH stretching region was initiated by Lee and coworkers (17, 18) and its rotational resolved spectra were then studied by Miller and coworkers (19), using IR predissociation spectroscopic methods. Saykally and coworkers carried out the far-IR absorption spectroscopy of neutral water clusters of different sizes, which provided detailed information on the structure and tunneling of these clusters (20–24). IR spectroscopy of size-selected neutral water clusters was also studied by Huisken et al., in which size selection was achieved by the rare-gas scattering method, followed by electron impact ionization (25). Vibrational spectra of neutral water hexamer were studied by Johnson and coworkers using argon-mediated, population-modulated electron attachment spectroscopy (26). IR-UV double-resonance spectroscopy of size-selected neutral water clusters attached by a benzene molecule was investigated by Zwier and coworkers (27, 28), and similar study on water clusters attached by a sodium atom was also performed (29). In 2012, Pate and coworkers identified the cage, prism, and book isomers of the water hexamer using the broadband microwave spectroscopy (30). Subsequently, concerted

Significance

Spectroscopic investigation of neutral water clusters is critical in understanding the structures and properties of condensed-phase water. Because of the difficulty for size selection of neutral clusters in general, infrared spectroscopic study of structural evolution of confinement-free, neutral water clusters has been a grand challenge. In this work, we exploit recently developed, hybrid instruments that integrate infrared spectroscopy with a tunable vacuum ultraviolet free-electron laser to capture structural evolution of water clusters. Striking spectral change in the OH stretch region is observed from water tetramer to penta- and hexamer, due to appearance of three-dimensional hydrogen-bonding networks. The technique has the potential to obtain the infrared spectra of size-selected neutral clusters and to access their rich structural landscape.

Author contributions: L.J., J.L., and X.Y. designed research; B.Z., Y.Y., Y.-Y.Z., S.J., Q.L., G.L., Z.Z., C.W., H.X., W.Z., D.D., G.W., D.H.Z., L.J., J.L., and X.Y. performed research; H.-S.H., D.H.Z., L.J., J.L., and X.Y. analyzed data; and L.J., J.L., and X.Y. wrote the paper.

The authors declare no competing interest.

This article is a PNAS Direct Submission.

Published under the PNAS license.

[1]B.Z., Y.Y., and Y.-Y.Z. contributed equally to this work.

[2]To whom correspondence may be addressed. Email: ljiang@dicp.ac.cn, junli@tsinghua.edu.cn, or xmyang@dicp.ac.cn.

This article contains supporting information online at https://www.pnas.org/lookup/suppl/doi:10.1073/pnas.2000601117/-/DCSupplemental.

First published June 15, 2020.

Downloaded at Dalian Inst Chemical Physics on October 9, 2020

quantum-tunneling-induced hydrogen-bond breaking in the neutral prism hexamer was investigated (31). Along with significant advances in theoretical calculations (32–36), these studies provided great insights into the hydrogen bonding structures and dynamics of neutral water clusters.

As pointed out by Clary (3), water molecules in liquid are held together by an ever-changing network of hydrogen bonds, which are 3D in nature. From previous studies, it is known that the water trimer, tetramer, and pentamer all have cyclic minimum-energy structures with all oxygen atoms in a two-dimensional (2D) plane, while the water hexamer has noncylic 3D structures (34–36). Clearly there are two important issues: when does the 2D-to-3D structural change occur in neutral water clusters and how is this structural change manifested in the OH stretching spectra? While it can provide crucial knowledge on hydrogen-bonding networks, size-specific IR spectroscopic study of confinement-free neutral water clusters in the OH stretch region has been very difficult because of the lack of proper tools for the size-selected probe of neutral clusters in general.

Recently, we have developed an intense tunable vacuum UV free-electron laser (VUV-FEL) facility (37), which provides a powerful tool for size-selective soft ionization for neutral clusters. This makes it possible to study the IR predissociation spectroscopy of confinement-free neutral water clusters using the IR-VUV scheme. In this work, we have systematically investigated the size-specific IR spectra of neutral water clusters, $(H_2O)_n$ (n = 3–6), using this IR-VUV scheme. Quantum-chemical studies were also carried out in an effort to understand the structural and spectral changes in these clusters.

The experimental study was carried out using an IR-VUV double-resonance spectroscopy apparatus at the VUV-FEL facility (38). In the experiment, neutral water clusters were generated by supersonic expansions of water vapor seeded in helium using a high-pressure pulsed valve (Even-Lavie valve, EL-7–2011-HT-HRR) that is capable of producing very cold molecular-beam conditions (39). The extraction plates of reflectron time-of-flight mass spectrometer (TOF-MS) were powered by a high-voltage direct current (dc) of 2,950 V. Charged clusters were deflected out of the molecular beam by the dc electric field of the extraction plates. Neutral water clusters in the beam were then threshold-ionized by the VUV-FEL pulse and mass-analyzed in the reflectron TOF-MS. The tunable IR laser pulse from an optical parametric oscillator was introduced at about 30 ns prior to the VUV-FEL pulse in the same VUV-FEL interaction region. When the IR laser frequency was resonant with a vibrational transition of a selected neutral cluster, vibrational predissociation caused the depletion of neutral cluster VUV ionization signal. The IR spectra of this size-selected neutral cluster were then recorded by monitoring the depletion of the signal intensity, $(H_2O)_n^+$, for a specific water cluster as a function of IR wavelength. Although the experimental temperature is not at 0 K, the rotational temperature should be less than 10 K, while the vibrational temperature of clusters could be much higher (i.e., a finite temperature), because vibrations are not easily cooled as rotation in our equipment.

Results

Fig. 1 shows the measured IR spectra of $(H_2O)_n$ (n = 3–6) in the OH stretching vibration region using the experimental method described above and the observed vibrational transitions are listed in Table 1. VUV wavelength and beam conditions were optimized to maximize the signal of a size-specific water cluster of interest with no interference from larger clusters (*SI Appendix*, Fig. S1). IR power dependence of the signal was measured to ensure that the predissociation yield is linear with photon flux. As shown in Fig. 1, the IR spectra of each individual cluster $(H_2O)_n$ (n = 3–6) in the OH stretching region are all different from each other, indicating that these IR spectra were measured at optimum experimental conditions with negligible contribution from larger clusters. The comparison of present VUV-FEL–based IR spectra of $(H_2O)_n$ (n = 4–6) with previous IR–molecular-beam spectra of $(H_2O)_n$ and IR-UV spectra of benzene-$(H_2O)_n$ is shown in *SI Appendix*, Fig. S2. The characteristic features of OH vibrational modes are well resolved in the VUV-FEL–based IR spectra of $(H_2O)_n$, revealing the remarkable evolution with cluster size.

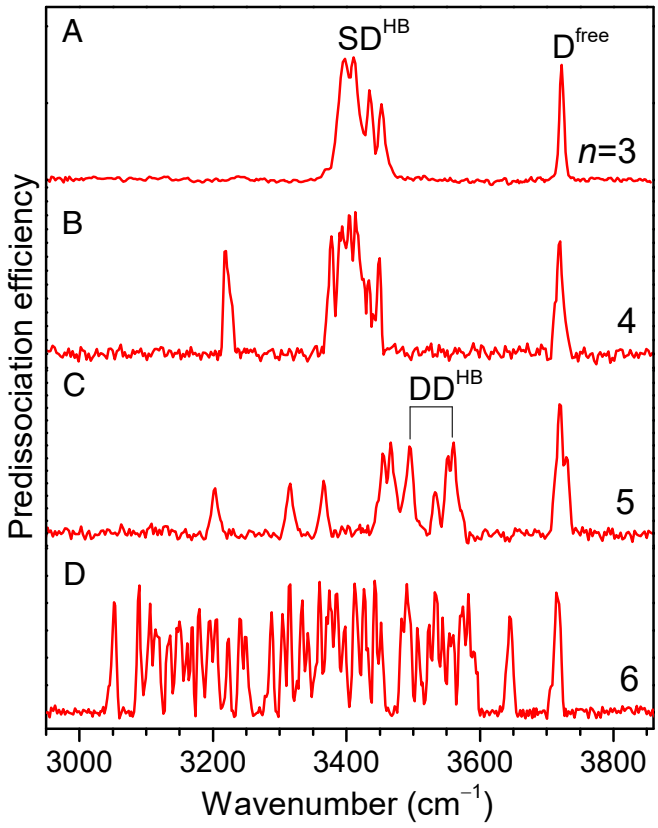

Fig. 1. IR spectra of neutral $(H_2O)_n$ clusters (A–D) with n = 3–6 in the OH stretch region.

Discussion

The experimental IR spectra of $(H_2O)_n$ (n = 3–6) can be classified as three groups of bands (Fig. 1 and Table 1), which are assigned by comparison with the previous studies (18, 19, 25, 27, 40, 41). The donor-free OH stretch (D^{free}) appears at 3,722 cm^{-1} in the IR spectrum of n = 3 and is slightly redshifted from 3,720 to 3,715 cm^{-1} for n = 4–6, similar to the virtually unchanged positions with cluster size in benzene-$(H_2O)_n$ (27). The OH stretch of water with single hydrogen-donor configuration (single-donor hydrogen-bonded OH stretch, labeled as SD^{HB}) shows quartet bands at 3,398, 3,410, 3,434, and 3,452 cm^{-1} for n = 3 and is considerably redshifted for n = 4–6.

The most striking observation in the present work is the IR spectrum of the pentamer in the OH stretch region (Fig. 1*C*), which is very different from those of the trimer and tetramer (Fig. 1 *A* and *B*). The IR spectrum of $(H_2O)_5$ shows distinct transitions at 3,494, 3,532, 3,553, and 3,561 cm^{-1}, which are characteristic of the OH stretch of water molecule with double hydrogen-donor configuration (double-donor hydrogen-bonded OH stretch, labeled as DD^{HB}) associated with the formation of a more compact, noncyclic structure (27, 40). The observed IR spectrum of $(H_2O)_6$ continues to exhibit the features of DD^{HB}, which becomes more complex and enormously spreads in the 3,000–3,700-cm^{-1} region. Consistent with the general observation, the OH stretch vibrational frequencies of double hydrogen-donor

Downloaded at Dalian Inst Chemical Physics on October 9, 2020

Table 1. The centroid frequencies of observed vibrational bands (in cm^{-1}) in $(H_2O)_n$

Label	$n = 3$	$n = 4$	$n = 5$	$n = 6$	Assignment
D^{free}	3,722	3,720	3,729	3,715	Donor-free OH stretch
			3,719		
SD^{HB}	3,452	3,450	3,466	3,000 ~ 3,450	Single-donor hydrogen-bonded OH stretch
	3,434	3,414	3,454		
	3,410	3,404	3,366		
	3,398	3,394	3,316		
		3,377	3,203		
DD^{HB}			3,561	3,450~ 3,650	Double-donor hydrogen-bonded OH stretch
			3,553		
			3,532		
			3,494		

water lie between those of donor-free water and single hydrogen-donor water (25, 27, 40).

To understand the hydrogen-bonding structures of these neutral water clusters and their IR spectra, theoretical studies were carried out for the low-lying isomers using the constrained basin-hopping global minimum search (42) and *ab initio* second-order Møller-Plesset/aug-cc-pVDZ (MP2/AVDZ) method. Relative energies were also calculated using the domain-based local pair natural orbital coupled cluster theory with single, double, and perturbative triple excitations/aug-cc-pVTZ (DLPNO-CCSD(T)/AVTZ) method at the MP2/AVDZ optimized geometries (see *SI Appendix* for computational details). The lowest-energy structures identified for neutral water clusters $(H_2O)_n$ ($n = 3$–6) are shown in *SI Appendix*, Fig. S3. Both calculations indicate that the most stable structure of the water trimer, tetramer, and pentamer are cyclic, whereas that of the hexamer is noncyclic, consistent with previously well-established threshold of 3D water structures instigating at hexamer (34–36). Vibrational frequencies for these neutral water clusters were also calculated using harmonic model at the MP2 level. For the $n = 3$ and 4 water clusters, the calculated harmonic vibrational stick spectra are in qualitative agreement with the experimental features (*SI Appendix*, Fig. S4). The detailed features in the experimental spectra of these clusters are, however, not exactly reproduced by the harmonic model at the MP2 level due to approximation in electron correlation and anharmonicity (25, 27).

The lowest-energy isomer calculated for the water pentamer (**5A**) remains cyclic with all oxygen atoms in the same 2D plane, in which each water molecule donates one hydrogen atom to form a single hydrogen bond with an adjacent water molecule (Fig. 2). In addition, there are also two more low-energy pentamer isomers, with the **5B** isomer lying at 1.1 kcal/mol and the **5C** isomer at 1.5 kcal/mol above the lowest-energy **5A** isomer. The **5B** and **5C** isomers have similar 3D structure to each other and can be viewed as a cyclic tetramer with an extra water vertically attached, in which the extra water molecule has double-donor hydrogen bonds with two adjacent water molecules. Vibrational stick spectra were calculated for these low-energy pentamer isomers. By comparison between experiment and theory (Fig. 2), the rather broad spectral feature of the free OH band, with a shoulder at the high-frequency side, shows that the 3D pentamer is present due to the low yet finite temperature. The calculated spectrum of the cyclic pentamer (**5A**) is very simple and clearly unable to explain the spectral features between 3,400 and 3,600 cm^{-1}, but these features match rather well with those of the low-energy 3D isomers, **5B** and **5C**. It thus appears that our technique is capable to trap both the global-minimum and low-lying isomers so that the cyclic and noncyclic pentamers can coexist to contribute to the experimental spectrum. Gibbs free-energy calculations show that the population of 5A and 5B/5C isomers hardly changes at the low-temperature range (*SI Appendix*, Fig. S5). Note that the experimental intensities of the DD^{HB} bands are stronger than those of the SD^{HB} bands, which might be due to the mode-specific predissociation efficiency upon IR laser radiation. Analogous difference in the IR spectral intensities of the DD^{HB} and SD^{HB} bands has also been found in the benzene-$(H_2O)_n$ clusters (27, 28).

The possible appearance of noncyclic pentamer, a higher-energy isomer than the cyclic pentamer previously characterized in the gas phase (23, 25), is quite interesting since no experimental evidence of noncyclic pentamer has ever been observed thus far. Previous molecular-dynamics simulations indicated that the water pentamer is seen to consist of multiple local minima separated by barriers below 60 K (43). Our MP2/AVDZ

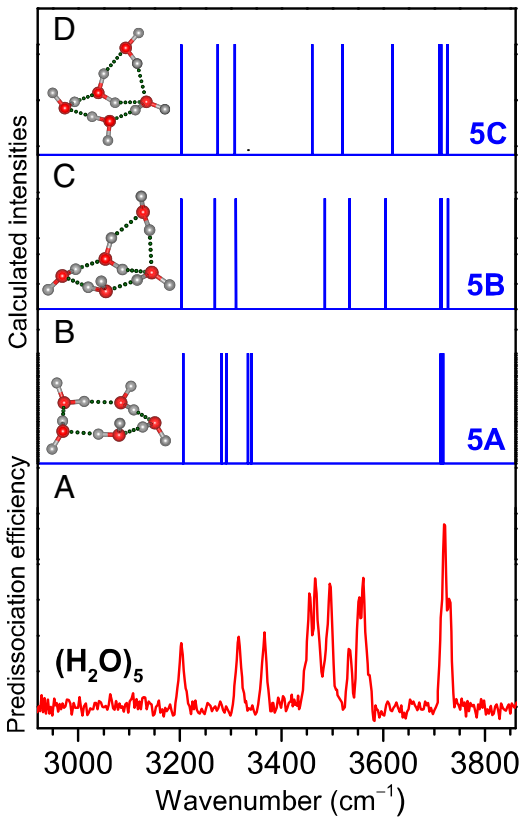

Fig. 2. Comparison of the experimental (*A*) and calculated (*B*–*D*) IR spectra of water pentamer, $(H_2O)_5$. Calculations were performed at the MP2/AVDZ level, with the harmonic frequencies scaled by 0.956. The structures of the **5A**, **5B**, and **5C** isomers are embedded in the inset.

Downloaded at Dalian Inst Chemical Physics on October 9, 2020

calculation shows that the interconversion barrier between the cyclic and noncyclic pentamers is ~1 kcal/mol. At the same theoretical level, the benzene-**5B** structure is calculated to be 1.5 kcal/mol higher in energy than the benzene-**5A** structure, indicating the noncyclic water structure becomes less stable when the benzene is tagged onto the water pentamer, which is consistent with the absence of noncyclic pentamer in the IR-UV spectroscopy of benzene-water clusters (27). The coexistence of cyclic and noncyclic pentamers in the present experiment might be explained by a kinetic mechanism that involves low-energy collisions between the cluster and the carrier gas atoms in the supersonic expansion (44). The formation of a short-lived complex with a collision partner increases the internal energy by the complex binding energy. When the internal energy of the transient complex is higher than the barriers separating different isomers, collision with carrier gas can induce isomerization to a lower-energy structure. It is known that the binding energy of a rare-gas atom with the complex follows the order of helium < neon < argon, mirroring an extent of the cooling efficiency (44). A particularly vivid example is that multiple coexisting structures of the cage, prism, and book hexamers were identified in the helium and neon expansions, whereas only the cage isomer, a nearly isoenergetic structure of prism isomer, was observed in an argon expansion (30). Interestingly, the high-energy cyclic hexamer was selectively formed in helium droplets under a different cluster growth condition (45). Higher-energy isomers on the potential energy surfaces of several neutral cluster systems were also kinetically trapped in helium (44, 46).

The IR spectrum of the hexamer (Fig. 1*D*) is significantly more complicated and covers much broader spectral range than all these smaller clusters studied here. Previous broadband microwave spectroscopy has identified the various hexamer isomers such as the prism, cage, and book isomers (30); therefore, the IR spectra of these isomers should all be present in the measured spectra. According to quantum-chemical calculations at the MP2 level, the most stable hexamer isomer is the prism structure, and other low-lying isomers identified are cage, book, bag, and cyclic isomers with calculated energy at 0.1, 0.2, 0.6, and 1.7 kcal/mol above the prism isomer (*SI Appendix*, Fig. S3), respectively. These calculated results are consistent with previous experimental observations (30).

The vibrational stick spectra of the three lowest-energy isomers of the hexamer are calculated and shown in *SI Appendix*, Fig. S6. The experimental OH stretching vibrational spectrum of the hexamer consists of at least 40 vibrational bands. Because of the existence of multiple isomers and difficulty in accurately calculating the IR spectra, the assignment of all of the vibrational bands for the hexamer is cumbersome. The signature free OH stretching peak at 3,715 cm^{-1} can be related to at least the three lowest-energy isomers, whereas the next highest-frequency assignable feature is the peak at 3,640 cm^{-1}, which seems to match the calculated peak of the double-donor hydrogen-bonded antisymmetric OH stretch for the prism isomer (labeled "*" in *SI Appendix*, Fig. S6). The lowest-frequency peak in the spectra at 3,050 cm^{-1} is likely to come from the single-donor OH stretch vibration of the prism isomer (labeled "◇" in *SI Appendix*, Fig. S6). While the observed vibrational bands of the hexamer are complex, most observable peaks can find rather good matches with the calculated vibrational bands for the three lowest-energy isomers that have been previously detected in the molecular beam (30). The calculated total vibrational stick spectra including the prism, cage, and book isomers are also shown in *SI Appendix*, Fig. S6, which cover the spectral region of 3,000–3,700 cm^{-1} of the hexamer and describe its vibrational spectral complexity. The OH stretch spectra of the water hexamer have been calculated at finite temperatures, which show an interesting progression from the cage spectrum at low temperatures to spectra of mixtures of isomers at higher temperatures (47).

The observed OH stretching vibrational spectra of the pentamer and hexamer are compared with that of liquid water in Fig. 3. Strikingly, their OH vibrational bands span the entire OH stretching vibrational bands of liquid water. The resemblance between IR spectra of the pentamer/hexamer and that of liquid water is quite remarkable. This suggests that hydrogen-bonding networks represented by the coexisting isomers of pentamer and hexamer at finite temperature can already describe the essential characteristics of the 3D hydrogen-bonding networks in liquid water.

As pointed out above, the lowest-energy isomers for the water trimer, tetramer, and pentamer are all cyclic structures, with all oxygen atoms on a 2D plane, while the lowest-energy structure of the hexamer is the prism structure with oxygen atoms in a 3D configuration (Fig. 4*A*). For the water pentamer, the low-lying 3D structure can coexist with the lowest-energy cyclic isomer. This interesting structural change is obviously due to the relative stability of the hydrogen-bonding networks in these clusters. Indeed, the calculated variation of adjacent O-O distances (R_{OO}) of the most stable structures with cluster size indicates the changeover starts to occur around $n = 5$ as well (Fig. 4*B*), which is also illustrated by the cross-over of the formation energies (*SI Appendix*, Fig. S7). The adjacent O-O distances along the O–H···O hydrogen bond is usually a good index to examine the trend in the intermolecular internal coordinates, which can be associated with statistical properties of condensed phases such as radial and angular distribution functions. Our MP2 calculations give an average R_{OO} value of 2.73 Å for the 2D structure of water pentamer (*SI Appendix*, Table S1), which is close to the value of 2.75 Å reported for ice (I_h) at 60 K (48). Furthermore, the MP2 $R_{O\text{-}O}$ value of 2.85 Å for the 3D structure of water pentamer (*SI Appendix*, Table S2) is the same as the value of 2.85 Å for liquid water at 298 K (49). These similarities suggest that the 2D and 3D structures of water pentamer play a significant role in

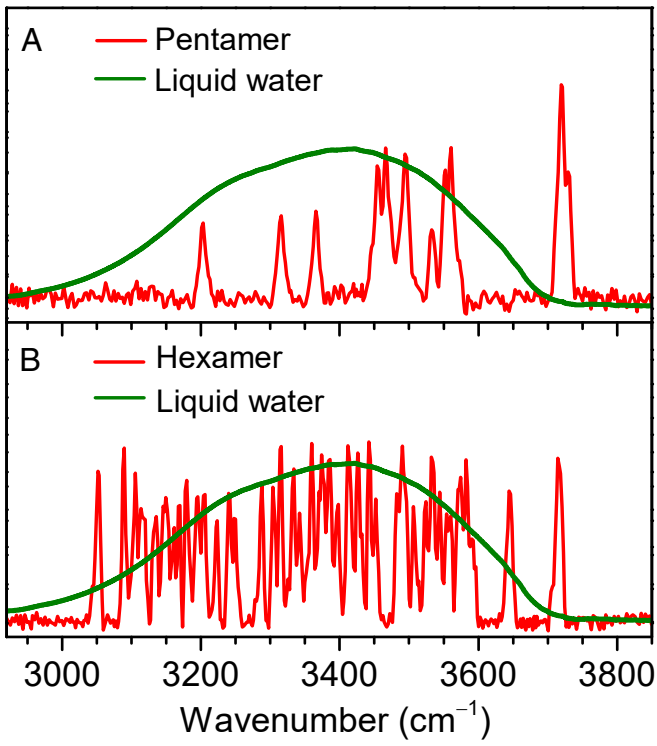

Fig. 3. Comparison of the experimental IR spectra of water pentamer (*A*) and hexamer (*B*) with that of liquid water at 298 K in the OH stretch region. The IR spectrum of liquid water at 298 K was recorded by a Fourier transform IR spectrometer.

Downloaded at Dalian Inst Chemical Physics on October 9, 2020

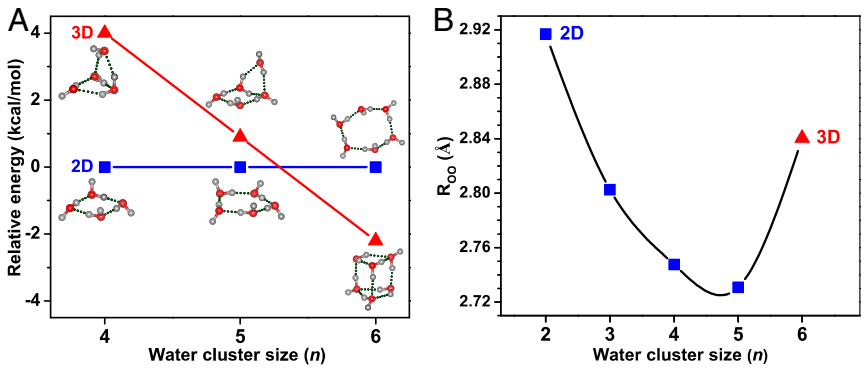

Fig. 4. (*A*) The structures and DLPNO-CCSD(T)/AVTZ relative energies of the most stable 2D and 3D isomers of $(H_2O)_n$ (n = 4–6) clusters. For pentamer the noncyclic isomer is energetically above the lowest-energy cyclic one but they coexist at finite temperature. (*B*) Change of the calculated O-O distances (R_{OO}) of the most stable 2D and 3D structures for $(H_2O)_n$ (n = 2–6) with cluster size. Square symbols stand for the 2D structures and triangle for the 3D structures shown in *SI Appendix*, Fig. S3.

accounting for the main features and the properties of liquid water as predicted by previous molecular-dynamics calculations (50–52).

To understand the bonding nature of the 2D-to-3D structural change, we analyzed the hydrogen-bonding network of water clusters using theoretical approaches of the molecular orbital theory, adaptive natural density partitioning (AdNDP) (53), and energy decomposition analysis–natural orbitals for chemical valence (54). As hydrogen bonding between a proton donor and an adjacent oxygen lone-pair acceptor (55) can be viewed as a multicenter interaction, AdNDP analysis can provide insight on the bonding feature. Indeed the AdNDP results show clearly a three-center two-electron (3c2e) interaction featuring the O lone pair delocalizing to the H–O bond region (*SI Appendix*, Fig. S8), in addition to the nominal 1c2e lone pairs, 2c2e donor-free O–H σ bonds, and the O–H bonds along the hydrogen-bond axis, respectively. The contribution of 3c2e hydrogen-bonding energy to the intrinsic total binding energy (E_{HB}/E_{total}) for the most stable 2D and 3D structures as a function of the cluster size is shown in *SI Appendix*, Fig. S9, which indicates that the contribution of 3c2e hydrogen bonding is saturated around $n = 5$ for the 2D isomers. For $(H_2O)_6$, the E_{HB}/E_{total} value of the prism structure (89.58%) is noticeably larger than that of the cyclic structure (87.22%), revealing the relatively high stability of the 3D prism structure. Note that the most stable 3D structures of $(H_2O)_5$ and $(H_2O)_6$ have six and nine hydrogen bonds, whereas their 2D cyclic structures only have five and six hydrogen bonds, respectively. These results point to the tendency for formation of the 3D structure for water pentamer and larger clusters and are consistent with the experimental OH stretch spectra of water pentamer and hexamer, which shows that the 3D structure becomes only slightly higher in energy than the 2D cyclic one starting at $(H_2O)_5$ and becomes dominant for $(H_2O)_6$. At finite temperature the low-lying and lowest-energy isomers of $(H_2O)_5$ can coexist, as is the case for $(H_2O)_6$.

In summary, the VUV-FEL–based IR spectroscopy of size-selected neutral water clusters yields unprecedented structure in their vibrational predissociation spectra. Striking spectral change in the OH stretch region was observed from water tetramer to hexamer, which is attributed to the appearance of 3D hydrogen-bonding networks at pentamer and hexamer at finite temperature. The present finding provides a consistent picture for the structural diversity of the hydrogen-bonding networks that are responsible for the major features of the structures and properties of condensed-phase water. The experimental data may stimulate further structural characterization of neutral water clusters and benchmark of spectroscopic theoretical methods.

Materials and Methods

A brief description of experimental and theoretical methods is given below. Further details and additional figures are provided in *SI Appendix*. In the experiment, water clusters were generated in a high-pressure supersonic expansion of a water–helium mixture. For the IR excitation of the clusters, we used a tunable IR optical parametric oscillator/optical parametric amplifier system (LaserVision) pumped by an injection-seeded solid-state laser (Continuum Surelite EX). Subsequent photoionization was carried out with about 30-ns delay with a tunable VUV-FEL light delivered by the Dalian Coherent Light Source (DCLS) facility. IR spectra were recorded in the difference mode of operation (IR laser on–IR laser off). Theoretical studies were carried out for the low-lying isomers of water clusters using the constrained basin-hopping global minimum search and *ab initio* MP2/aug-cc-pVDZ method using the Gaussian G09 software package.

Data Availability. The procedures of experiments and simulations are described in detail in *Materials and Methods* and in *SI Appendix*. Data used for this paper are available in Supporting Information as Dataset S1.

ACKNOWLEDGMENTS. The authors gratefully acknowledge the DCLS for VUV-FEL beam time and the DCLS staff for support and assistance. This work was supported by the National Natural Science Foundation of China: Grant 21688102 (X.Y. and D.H.Z.); Grant 21673231 (L.J.), Grants 21590792 and 91645203 (J.L.); the Strategic Priority Research Program of Chinese Academy of Sciences (Grant XDB17000000); Dalian Institute of Chemical Physics (Grant DICP DCLS201702); International Partnership Program of Chinese Academy of Sciences (Grant No. 121421KYSB20170012); the Science Challenge Project (Project TZ2016004); K. C. Wong Education Foundation (GJTD-2018-06); and Guangdong Key Laboratory of Catalytic Chemistry. The calculations were performed on SUSTech supercomputer.

1. F. N. Keutsch, R. J. Saykally, Water clusters: Untangling the mysteries of the liquid, one molecule at a time. *Proc. Natl. Acad. Sci. U.S.A.* **98**, 10533–10540 (2001).
2. R. Ludwig, Water: From clusters to the bulk. *Angew. Chem. Int. Ed. Engl.* **40**, 1808–1827 (2001).
3. D. C. Clary, CHEMISTRY. Quantum dynamics in the smallest water droplet. *Science* **351**, 1267–1268 (2016).
4. J. C. Jiang *et al.*, Infrared spectra of $H^+(H_2O)_{5-8}$ clusters: Evidence for symmetric proton hydration. *J. Am. Chem. Soc.* **122**, 1398–1410 (2000).
5. M. Miyazaki, A. Fujii, T. Ebata, N. Mikami, Infrared spectroscopic evidence for protonated water clusters forming nanoscale cages. *Science* **304**, 1134–1137 (2004).
6. J. W. Shin *et al.*, Infrared signature of structures associated with the $H^+(H_2O)_n$ (n = 6 to 27) clusters. *Science* **304**, 1137–1140 (2004).
7. K. R. Asmis *et al.*, Gas-phase infrared spectrum of the protonated water dimer. *Science* **299**, 1375–1377 (2003).
8. J. M. Headrick *et al.*, Spectral signatures of hydrated proton vibrations in water clusters. *Science* **308**, 1765–1769 (2005).
9. J. A. Fournier *et al.*, Vibrational spectral signature of the proton defect in the three-dimensional $H^+(H_2O)_{21}$ cluster. *Science* **344**, 1009–1012 (2014).
10. J. A. Fournier *et al.*, Site-specific vibrational spectral signatures of water molecules in the magic H_3O^+ $(H_2O)_{20}$ and Cs^+ $(H_2O)_{20}$ clusters. *Proc. Natl. Acad. Sci. U.S.A.* **111**, 18132–18137 (2014).
11. C. T. Wolke *et al.*, Spectroscopic snapshots of the proton-transfer mechanism in water. *Science* **354**, 1131–1135 (2016).

Downloaded at Dalian Inst Chemical Physics on October 9, 2020

12. W. H. Robertson, E. G. Diken, E. A. Price, J. W. Shin, M. A. Johnson, Spectroscopic determination of the OH^- solvation shell in the $OH^-(H_2O)_n$ clusters. *Science* **299**, 1367–1372 (2003).
13. A. E. Bragg, J. R. R. Verlet, A. Kammrath, O. Cheshnovsky, D. M. Neumark, Hydrated electron dynamics: From clusters to bulk. *Science* **306**, 669–671 (2004).
14. N. I. Hammer *et al*., How do small water clusters bind an excess electron? *Science* **306**, 675–679 (2004).
15. J. R. R. Verlet, A. E. Bragg, A. Kammrath, O. Cheshnovsky, D. M. Neumark, Observation of large water-cluster anions with surface-bound excess electrons. *Science* **307**, 93–96 (2005).
16. K. R. Siefermann *et al*., Binding energies, lifetimes and implications of bulk and interface solvated electrons in water. *Nat. Chem.* **2**, 274–279 (2010).
17. M. F. Vernon *et al*., Vibrational predissociation spectra and dynamics of small molecular clusters of H_2O and HF. *Faraday Discuss.* **73**, 387–397 (1982).
18. R. H. Page, J. G. Frey, Y. R. Shen, Y. T. Lee, Infrared predissociation spectra of water dimer in a supersonic molecular beam. *Chem. Phys. Lett.* **106**, 373–376 (1984).
19. Z. S. Huang, R. E. Miller, High-resolution near-infrared spectroscopy of water dimer. *J. Chem. Phys.* **91**, 6613–6631 (1989).
20. N. Pugliano, J. D. Cruzan, J. G. Loeser, R. J. Saykally, Vibrational and K′ a dependencies of the multidimensional tunneling dynamics in the 82.6 cm^{-1} intermolecular vibration of the water dimer-d_4. *J. Chem. Phys.* **98**, 6600–6617 (1993).
21. N. Pugliano, R. J. Saykally, Measurement of quantum tunneling between chiral isomers of the cyclic water trimer. *Science* **257**, 1937–1940 (1992).
22. J. D. Cruzan *et al*., Quantifying hydrogen bond cooperativity in water: VRT spectroscopy of the water tetramer. *Science* **271**, 59–62 (1996).
23. K. Liu, M. G. Brown, J. D. Cruzan, R. J. Saykally, Vibration-rotation tunneling spectra of the water pentamer: Structure and dynamics. *Science* **271**, 62–64 (1996).
24. K. Liu *et al*., Characterization of a cage form of the water hexamer. *Nature* **381**, 501–503 (1996).
25. F. Huisken, M. Kaloudis, A. Kulcke, Infrared spectroscopy of small size-selected water clusters. *J. Chem. Phys.* **104**, 17–25 (1996).
26. E. G. Diken, W. H. Robertson, M. A. Johnson, The vibrational spectrum of the neutral $(H_2O)_6$ precursor to the "magic" $(H_2O)_6^-$ cluster anion by argon-mediated, population-modulated electron attachment spectroscopy. *J. Phys. Chem. A* **108**, 64–68 (2004).
27. R. N. Pribble, T. S. Zwier, Size-specific infrared spectra of benzene-$(H_2O)_n$ clusters (n = 1 through 7): Evidence for noncyclic $(H_2O)_n$ structures. *Science* **265**, 75–79 (1994).
28. C. J. Gruenloh *et al*., Infrared spectrum of a molecular ice cube: The S_4 and D_{2d} water octamers in benzene-$(water)_8$. *Science* **276**, 1678–1681 (1997).
29. C. C. Pradzynski, R. M. Forck, T. Zeuch, P. Slavíček, U. Buck, A fully size-resolved perspective on the crystallization of water clusters. *Science* **337**, 1529–1532 (2012).
30. C. Pérez *et al*., Structures of cage, prism, and book isomers of water hexamer from broadband rotational spectroscopy. *Science* **336**, 897–901 (2012).
31. J. O. Richardson *et al*., Concerted hydrogen-bond breaking by quantum tunneling in the water hexamer prism. *Science* **351**, 1310–1313 (2016).
32. R. Bukowski, K. Szalewicz, G. C. Groenenboom, A. van der Avoird, Predictions of the properties of water from first principles. *Science* **315**, 1249–1252 (2007).
33. J. M. Bowman, Y. Wang, H. Liu, J. S. Mancini, Ab initio quantum approaches to the IR spectroscopy of water and hydrates. *J. Phys. Chem. Lett.* **6**, 366–373 (2015).
34. B. Temelso, K. A. Archer, G. C. Shields, Benchmark structures and binding energies of small water clusters with anharmonicity corrections. *J. Phys. Chem. A* **115**, 12034–12046 (2011).
35. E. Miliordos, S. S. Xantheas, An accurate and efficient computational protocol for obtaining the complete basis set limits of the binding energies of water clusters at the MP2 and CCSD(T) levels of theory: Application to $(H_2O)_m$, m = 2-6, 8, 11, 16, and 17. *J. Chem. Phys.* **142**, 234303 (2015).
36. A. Rakshit, P. Bandyopadhyay, J. P. Heindel, S. S. Xantheas, Atlas of putative minima and low-lying energy networks of water clusters n = 3-25. *J. Chem. Phys.* **151**, 214307 (2019).
37. D. Normile, Unique free electron laser laboratory opens in China. *Science* **355**, 235 (2017).
38. B. Zhang *et al*., Infrared spectroscopy of neutral water dimer based on a tunable vacuum ultraviolet free electron laser. *J. Phys. Chem. Lett.* **11**, 851–855 (2020).
39. U. Even, J. Jortner, D. Noy, N. Lavie, C. Cossart-Magos, Cooling of large molecules below 1 K and He clusters formation. *J. Chem. Phys.* **112**, 8068–8071 (2000).
40. R. Knochenmuss, S. Leutwyler, Structures and vibrational spectra of water clusters in the self-consistent-field approximation. *J. Chem. Phys.* **96**, 5233–5244 (1992).
41. S. S. Xantheas, T. H. Dunning, Ab initio studies of cyclic water clusters $(H_2O)_n$ (n = 1-6). I. Optimal structures and vibrational spectra. *J. Chem. Phys.* **99**, 8774–8792 (1993).
42. X. Chen, Y.-F. Zhao, L.-S. Wang, J. Li, Recent progresses of global minimum searches of nanoclusters with a constrained Basin-Hopping algorithm in the TGMin program. *Comput. Theor. Chem.* **1107**, 57–65 (2017).
43. P. L. M. Plummer, T. S. Chen, Investigation of structure and stability of small clusters: Molecular dynamics studies of water pentamers. *J. Chem. Phys.* **86**, 7149–7155 (1987).
44. U. Erlekam, M. Frankowski, G. von Helden, G. Meijer, Cold collisions catalyse conformational conversion. *Phys. Chem. Chem. Phys.* **9**, 3786–3789 (2007).
45. K. Nauta, R. E. Miller, Formation of cyclic water hexamer in liquid helium: The smallest piece of ice. *Science* **287**, 293–295 (2000).
46. A. J. Minei, S. E. Novick, Microwave observation of the "recently found" polar OCS dimer. *J. Chem. Phys.* **126**, 101101 (2007).
47. C. J. Tainter, J. L. Skinner, The water hexamer: Three-body interactions, structures, energetics, and OH-stretch spectroscopy at finite temperature. *J. Chem. Phys.* **137**, 104304 (2012).
48. W. F. Kuhs, M. S. Lehmann, The structure of the ice I_h by neutron diffraction. *J. Phys. Chem.* **87**, 4312–4313 (1983).
49. A. H. Narten, W. E. Thiessen, L. Blum, Atom pair distribution functions of liquid water at 25°C from neutron diffraction. *Science* **217**, 1033–1034 (1982).
50. A. Rahman, F. H. Stillinger, Hydrogen-bond patterns in liquid water. *J. Am. Chem. Soc.* **95**, 7943–7948 (1973).
51. R. J. Speedy, J. D. Madura, W. L. Jorgensen, Network topology in simulated water. *J. Phys. Chem.* **91**, 909–913 (1987).
52. G. Corongiu, E. Clementi, Solvated water molecules and hydrogen bridged networks in liquid water. *J. Chem. Phys.* **98**, 2241–2249 (1993).
53. D. Y. Zubarev, A. I. Boldyrev, Developing paradigms of chemical bonding: Adaptive natural density partitioning. *Phys. Chem. Chem. Phys.* **10**, 5207–5217 (2008).
54. M. P. Mitoraj, A. Michalak, T. Ziegler, A combined charge and energy decomposition scheme for bond analysis. *J. Chem. Theory Comput.* **5**, 962–975 (2009).
55. A. E. Reed, F. Weinhold, Natural bond orbital analysis of near-Hartree-Fock water dimer. *J. Chem. Phys.* **78**, 4066–4073 (1983).

Downloaded at Dalian Inst Chemical Physics on October 9, 2020